

# Photoelectrochemical Investigation of an Azopyridinium Compound ((CH<sub>3</sub>)<sub>2</sub>NC<sub>6</sub>H<sub>4</sub>–N=N–C<sub>5</sub>H<sub>4</sub>NC<sub>18</sub>H<sub>37</sub>I) Modified SnO<sub>2</sub> Electrodes

W. S. Xia, C. H. Huang,\* C. P. Luo, L. B. Gan, and Z. D. Chen

State Key Laboratory of Rare Earth Material Chemistry and Applications, Peking University, Beijing, 100871, China

Received: March 28, 1996; In Final Form: June 13, 1996<sup>⊗</sup>

The steady photoelectric response of an azopyridinium compound, (CH<sub>3</sub>)<sub>2</sub>NC<sub>6</sub>H<sub>4</sub>–N=N–C<sub>5</sub>H<sub>4</sub>NC<sub>18</sub>H<sub>37</sub>I (AI), monolayer modified SnO<sub>2</sub> electrodes prepared by the Langmuir–Blodgett technique has been investigated using a conventional photoelectrochemical cell. Under ambient condition, a cathodic photocurrent is observed when the AI–SnO<sub>2</sub> electrode is illuminated by white light (the IR was filtered). The action spectrum is coincident with the absorption of the electrode in the region around 450 nm, indicating the AI aggregates in LB film are responsible for the photocurrent. Dependencies of the photocurrent on some factors have been studied, which may change the magnitude of the observed photocurrent, namely, the light intensity of the irradiation, the concentration of the donor or acceptor in electrolyte solution, bias voltage, and the saturation degree of O<sub>2</sub> or N<sub>2</sub>. Based on the changes of absorption spectra of AI in benzene solvent before and after irradiation, the electrochemical behaviors of AI in LB films are studied and the calculations of bond length, charge distribution, and total energy of different state for an analogue of AI, (CH<sub>3</sub>)<sub>2</sub>NC<sub>6</sub>H<sub>4</sub>–N=N–C<sub>5</sub>H<sub>4</sub>N<sup>+</sup>CH<sub>3</sub> (AM), were performed by using MINDO/3 method. The photocurrent generation is believed to result from photoinduced tautomerism upon irradiation.

## Introduction

There is much interest focused on designing artificial systems on various surfaces such as modified electrode, bilayer lipid membrane, liquid crystal, and LB films, etc.<sup>1–4</sup> to simulate the processes occurring in biological systems in which molecules organized themselves into functional entities, e.g. the photosynthetic unit. As one of these prospective techniques, Langmuir–Blodgett film may be used in constructing molecular electronic and photonic devices in future.<sup>5,6</sup> Photoinduced electron transfer reactions in LB films are among the most important process which may be controlled at the molecular level to achieve such purposes. In order to explore more effective photoelectric response systems, molecular designs have been concentrating on developing both intramolecular electron transfer reaction, in which an electron donor and an electron acceptor moiety are linked into one molecule with an alkyl chain or a rigid hydrocarbon spacer as with the folded type S-A-D or linear type A-S-D, etc., and intermolecular electron transfer reaction by depositing an electron donor or an electron acceptor with sensitizer in LB film through a sandwich depositing mode.<sup>4</sup> The mechanism of photoinduced electron transfer (PET) has been vigorously investigated from theoretical<sup>7</sup> and experimental<sup>8</sup> standpoints by many researchers on account of their potential uses in photoinduced charge storage<sup>9</sup> and photosynthetic prototype.<sup>10</sup> Although the detailed molecular arrangements and the film structures have not been well clarified, the characteristics of photoelectric energy conversion have been examined. As examples of these attributions, several artificial photoelectrochemically active systems in LB films such as merocyanine,<sup>11</sup> triad molecules,<sup>12</sup> squaraine,<sup>13</sup> Ru(bpy)<sup>3+</sup> derivative,<sup>14</sup> etc. have been investigated. It is found that quantum yields of these artificial systems were in the order of 10<sup>-4</sup>–10<sup>-3</sup>.

Azo compounds which have many good photoelectrochemical properties are one kind of potential materials which may be

used in the area of information storage,<sup>15</sup> nonlinear optics,<sup>16</sup> photochemical switch,<sup>17</sup> etc. Basic studies on this kind of compounds are very valuable in “molecular engineering”. Since aromatic chromophores have  $\pi$ -electron which may facilitate the electron transfer reaction between donors and acceptors linked by them as bridge,<sup>18,19</sup> it is anticipated that such molecular structure with a strong polarity effect may produce considerable photoelectric response signals. On the basis of this thought, we first reported a highly polar azopyridinium compound, (CH<sub>3</sub>)<sub>2</sub>NC<sub>6</sub>H<sub>4</sub>–N=N–C<sub>5</sub>H<sub>4</sub>NC<sub>18</sub>H<sub>37</sub>I (AI), which has an electron donor–dimethylamino group and an electron acceptor–positive pyridinium ion linked by a rigid  $\pi$ -conjugated system as an electron bridge. Since this highly polar molecule can form intramolecular charge transfer complex easily, it is very interesting to study its photochemical behaviors which may have potential uses in the area of photoelectric conversion, photochemical switch, and the electron transfer mechanism within a molecule itself. Although photoelectrically active bilayer lipid membrane (BLM) shows strong potential in the construction of biological electronic devices (BED),<sup>20</sup> solving its stability is an urgent problem facing scientists. In order to overcome the extreme fragility of the BLM and avoid the limitation of the solubility of the photosensitizer in the supporting material of the BLM and also to increase the numbers of sensitizer molecules per unit area, in the present study, we have used the Langmuir–Blodgett technique to deposit AI on a SnO<sub>2</sub> substrate. A photocurrent is observed when the film is irradiated and the quantum yield is about 10<sup>-2</sup>, considerably larger than some of the artificial photoelectric systems in LB films. The good correspondence of the action spectrum of AI with the UV–vis absorption of AI on SnO<sub>2</sub> electrode suggests that the aggregates in LB films are responsible for the photocurrent generation. From various photochemical reactions of AI in solution or in LB film and the quantum chemical calculations, a possible mechanism for the photoconductive phenomenon is also proposed.

\* To whom correspondence should be addressed.

<sup>⊗</sup> Abstract published in *Advance ACS Abstracts*, August 15, 1996.

## Experimental Section

**Materials.** The synthesis and characterization of AI have been reported elsewhere.<sup>16</sup> Methyl viologen diiodide (MV<sup>2+</sup>) was synthesized by the reaction of 4,4'-dipyridyl with excess methyl iodide in refluxing ethanol for 6 h. The product was filtered and then washed by ethanol for four times and its purity was characterized by <sup>1</sup>H NMR and elemental analysis. The pure water was in-house deionized water purified by passing through an EASYpure RF compact ultrapure water system (Barnstead Co., USA) and the resistivity is over  $18 \times 10^6 \Omega \cdot \text{cm}$ . All other reagents were of analytical grade and were used without further purification except hydroquinone (HQ) which was recrystallized from water before use. AA represents ascorbic acid.

**$\pi$ -A Isotherms and Film Deposition.** The monolayers of AI were formed by dropping its CHCl<sub>3</sub> solution ( $\sim 0.5 \text{ mg/mL}$ ) on a pure water subphase ( $20 \pm 1 \text{ }^\circ\text{C}$ , pH 5.6) or 0.1 mol/L NaI aqueous solution subphase on a British NIMA Technology Langmuir-Blodgett Model 622 trough. After vaporization of CHCl<sub>3</sub>, the surface pressure-area ( $\pi$ -A) isotherms were recorded. Transparent SnO<sub>2</sub> glass substrates with a lateral resistance of  $10 \text{ ohms} \cdot \text{cm}^{-1}$  were hydrophilically pretreated. The LB films were fabricated by dipping the substrate into the aqueous subphase and raised at a rate of  $5 \text{ mm/min}$  with a moderate surface pressure ( $35 \text{ mN/m}$ ). The multiple layers are deposited in Y-type mode. The transfer ratios were about 1.

**Electrochemical Measurements.** The conventional three-electrode setup with a  $0.8 \text{ cm}^2$  effective contact area was used for all irradiation experiments. The film-modified SnO<sub>2</sub> glass was used as a working electrode (WE), a Pt electrode as a counter electrode (CE), and a Ag/AgCl electrode as a reference electrode (RE). The electrolyte solution for the measurement of photocurrent was 1 mol/L KCl aqueous solution. Another electrolyte solution for electrochemical measurement was the Britton-Robinson buffer solution (pH 2–10) containing 1 mol/L KCl. The Britton-Robinson buffer solution consists of acetic acid, phosphoric acid, boric acid, and hydroxide sodium. Before every measurement of cyclic voltammetry, the electrolyte solution was deaerated with high-purity N<sub>2</sub> gas for 5 min. All measurements were made at room temperature on a Model 600 voltammetric analyzer (CH Instruments, USA). The different concentrations of donor or acceptor in electrolyte solution are obtained by adding solid sample into the solution directly.

**Photochemical Experiments.** A 500 W xenon lamp (Ushio Electric, Japan) was used as the excitation source for the photochemical experiments. Different wavelengths were obtained by using various filter with a certain band-pass, for instance, the absorption centered at 450 nm (Toshiba KL-45, Japan) with a half band-pass of 15 nm. The intensity of incident beam was checked up by model LM-91 Photopower meter (National Institute of Metrology, Beijing, China). The IR light was filtered for all the experiments with Toshiba IRA-25S filter (Japan).

**Spectroscopic Measurement.** The UV-vis spectra were recorded on a Shimadzu UV-3100 spectrometer (Japan).

**Quantum Chemical Calculation.** MINDO/3 calculation method from Ceris<sup>2</sup> software was adopted in HP9000/720(PA-RISC) workstation. In order to make the calculation more easy, we selected a model molecule [(CH<sub>3</sub>)<sub>2</sub>NC<sub>6</sub>H<sub>4</sub>-N=N-C<sub>5</sub>H<sub>4</sub>N<sup>+</sup>-CH<sub>3</sub> (AM)] with a short tail methyl to replace the longer tail octadecyl group in AI.

## Results and Discussions

**Fabrication of AI-SnO<sub>2</sub> Electrode.** The title compound AI can form stable monolayers both on pure water surface and 0.1 mol/L NaI aqueous solution surface. The slope of their

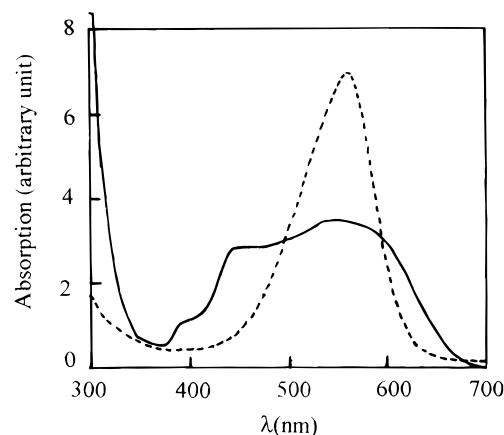
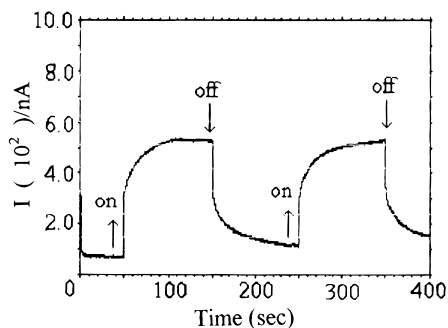


**Figure 1.** Absorption spectra of AI in SnO<sub>2</sub> electrode (—) and that in CHCl<sub>3</sub> solvent (---).

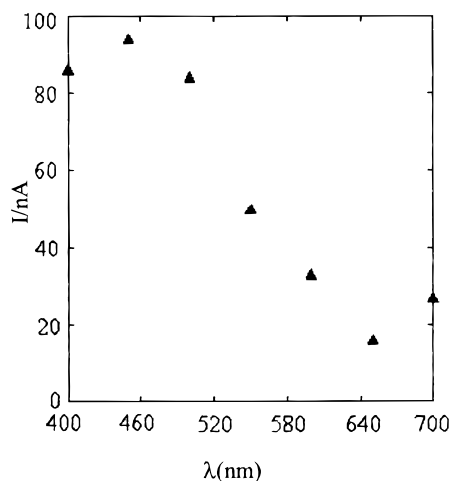
isotherms is about the same,  $\sim -3.0 \text{ mN} \cdot \text{m}^{-1} \cdot \text{Å}^{-2}$ , but their collapse pressure is not identical,  $58.7 \text{ mN/m}$  for the former and  $65 \text{ mN/m}$  for the latter. Furthermore, the solid phase region can be extended from  $10.7$ – $58.7 \text{ mN/m}$  in pure water subphase to  $6.7$ – $65 \text{ mN/m}$  in 0.1 mol/L NaI aqueous subphase. All these facts indicate that the film formation properties are improved with the presence of I<sup>-</sup> ions in the subphase. Comparing with the area per molecule of AI in the two cases, a difference about  $6 \text{ Å}^2$  between them is observed. For the former the area per molecule is  $36 \text{ Å}^2$  and for the latter the area per molecule is  $42 \text{ Å}^2$ , indicating that I<sup>-</sup> ions occupy a certain space in the formation of the film. Since I<sup>-</sup> is relatively large (the radius is about  $2 \text{ Å}$  and the section area is about  $12 \text{ Å}^2$ ), it may sustain the molecules to stand perpendicularly to the electrode surface resulting in better film formation. In addition, I<sup>-</sup> ions existing in the subphase may decrease the solubility of AI due to the co-ions effect.

Figure 1 shows the absorption spectrum of AI on SnO<sub>2</sub> electrode and that in CHCl<sub>3</sub> solvent. Both spectra have an absorption at 560 nm which may be attributed to the  $\pi \rightarrow \pi^*$  transition of -N=N- group. However, the absorption of AI on SnO<sub>2</sub> electrode shows a broad absorption. The absorption at 450 nm which has 110 nm blue shift compared with 560 nm may result from the interaction of the packed azo groups in the LB film, the formation of H-aggregates<sup>21</sup> in LB film. The absorption centered at 560 nm in the LB film may be contributed by the absorption of monomeric AI. The broad absorption is a mixture of these two kinds of existing state on the AI-SnO<sub>2</sub> electrode. In order to prove the correctness of the above assignment, we used a lower polar solvent, benzene, to substitute chloroform as the spread solution. As a result, the absorption spectrum of AI monolayer on SnO<sub>2</sub> electrode prepared from benzene solution also shows a broad absorption with a shoulder absorption at 450 nm. Therefore, the blue shift of the absorption may result from the formation of aggregates, rather than the change of solvent polarity.

**Photocurrent Generation from AI-SnO<sub>2</sub> Electrodes.** A steady cathodic photocurrent is observed when the AI-SnO<sub>2</sub> electrode is illuminated by white light or 450 nm as shown in Figure 2. Among the more than 20 parallel data resulting from AI-SnO<sub>2</sub> electrodes, the photocurrent observed ranges from 380 to 580 nA in 1 mol/L KCl electrolyte solution without any bias voltage under a light intensity of  $240 \text{ mW/cm}^2$  (white light) corresponding with an open circuit voltage ( $V_{oc}$ ) of  $\sim 160 \text{ mV}$ . The film shows a very stable photoelectric response for tens of times of switching on and off the light. In order to identify the contribution of SnO<sub>2</sub> to photocurrent, three independent uncoated SnO<sub>2</sub> electrodes were tested. It was found that an anionic



**Figure 2.** Photocurrent generation from AI-SnO<sub>2</sub> electrode upon irradiation of white light at 240 mW/cm<sup>2</sup>.



**Figure 3.** Action spectrum of AI-SnO<sub>2</sub> electrode. The intensities of different wavelengths were all normalized.

photocurrent about 20 nA could be observed when uncoated SnO<sub>2</sub> was used as electrode in the same electrolyte solution upon irradiation of 240 mW/cm<sup>2</sup> white light. While using 450 nm irradiation, no photoresponse was observed from the uncoated SnO<sub>2</sub> electrode (the reason is that the absorption of SnO<sub>2</sub> is below 350 nm). A photocurrent of 120–150 nA was obtained in 1 mol/L KCl electrolyte solution without bias at 450 nm irradiation ( $1.8 \times 10^{16}$  photons/(cm<sup>2</sup>·s)), so the quantum yield, which is cited per absorbed photon, is about 0.14% (the absorbency ratio of the monolayer on the SnO<sub>2</sub> electrode at 450 nm is about 4%). To test the stability of AI monolayer modified SnO<sub>2</sub> electrode, we selected three such electrodes submerged in 1 mol/L KCl electrolyte solution. At the first 5–6 days, the photocurrent remained almost unchanged and then decreased gradually at a rate of 1 nA per day in the testing range of 1 month.

Figure 3 shows the action spectrum of AI on SnO<sub>2</sub> electrodes. The most effective wavelength centers at 450 nm. Comparing the action spectrum with the absorption spectrum (see Figure 1), we can see that the action spectrum is coincident with the absorption spectrum of AI on SnO<sub>2</sub> electrode very well in the region around 450 nm, suggesting that the aggregates of AI deposited in the LB film are responsible for the photocurrent generation. However, the monomeric AI molecules cannot generate photocurrent, indicating that electron transfer within aggregates is the key event subsequent to photoexcitation of aggregates.

**Effect of Bias Voltage and Light Intensity.** The observation of cathodic photocurrent indicates that electrons flow from the electrode through the LB film to the electrolyte solution. To further probe the electron-transfer process between the SnO<sub>2</sub> electrode and the LB film, the effect of bias voltage was

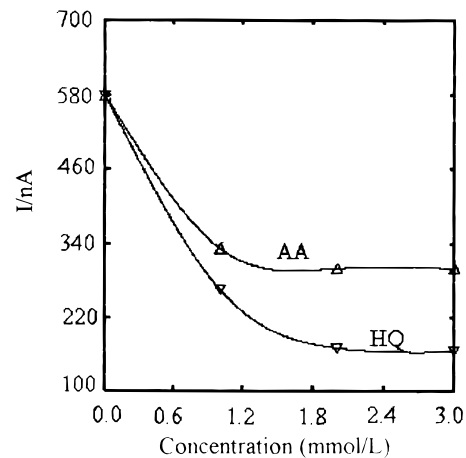


**Figure 4.** Dependence of photocurrent generation from AI-SnO<sub>2</sub> electrode with vitamin A (AA) and hydroquinone (HQ) in 1 mol/L KCl electrolyte solution upon irradiation of 240 mW/cm<sup>2</sup>.

investigated. There is a linear relationship between the observed photocurrent and the bias voltage with a slope of 2.25 nA/mV in the region of  $-0.4$ – $0.18$  V ( $\sim$ Ag/AgCl). An increase of the cathodic photocurrent with increasing negative bias to the electrode can be seen and vice versa. When the bias voltage is more negative than  $-0.4$  V, the photocurrent reaches a steady value and does not increase with the negative bias. On the other hand, when the bias voltage is more positive than 0.18 V, the photocurrent converse, an anionic photocurrent appearing. The reason may be that the applied negative voltage forms a strong electric field in the LB film which may accelerate the photo-induced electron-hole separation and the velocity of hole shift to the surface of SnO<sub>2</sub> and the electrons flowing to the electrolyte solution. This decreases the probability of capture of the photocarrier (electron) by recombination or “trapping” and lengthens the lifetime of charge separation.

For the AI-SnO<sub>2</sub> electrodes, it can be seen that the photocurrent increases linearly with the light intensity in the lower intensity range ( $<100$  mW/cm<sup>2</sup>), and it gradually reaches a saturation state in the higher intensity range ( $>240$  mW/cm<sup>2</sup>), suggesting that all the active molecules may contribute to the photocurrent at high light intensity.

**Effect of Electron Donor and Acceptor.** As expected, when the well-known electron acceptor, methyl viologen (MV<sup>2+</sup>) is added to 1 mol/L KCl electrolyte solution, a linear increase of photocurrent with the concentration of MV<sup>2+</sup> in electrolyte solution is observed. The increasing magnitude of photocurrent is about 50 nA with the addition of 1 mmol/L MV<sup>2+</sup> into 1 mol/L KCl solution without any bias voltage under irradiation of 240 mW/cm<sup>2</sup> white light. Contrarily, when the electron donors ascorbate acid (AA) and hydroquinone (HQ) were added to electrolyte solution, a sharp decrease of photocurrent at lower concentration and gradually to be saturated is seen in Figure 4. HQ is a relatively stronger photocurrent quencher than AA. HQ did not change the direction of the photocurrent here, unlike that observed in the squaraine system.<sup>13</sup>

Since O<sub>2</sub> can accept an electron to form a superoxide anion radical, it is a potential electron acceptor. The magnitude of photocurrent is 2-fold raised after the electrolyte solution is saturated by O<sub>2</sub> ([O<sub>2</sub>]  $\sim 1.2 \times 10^{-3}$  mol/L)<sup>13</sup> (about 5 min or longer ventilating) compared with the ambient condition, e.g., [O<sub>2</sub>]  $\sim 2.7 \times 10^{-4}$  mol/L.<sup>22</sup> However, when N<sub>2</sub> gas was used to degas the O<sub>2</sub> in electrolyte solution, the effect to the photocurrent is not significant. The decrease ratio of the photocurrent is smaller than 5% and it can be recovered after the old electrolyte solution is updated by a new one.

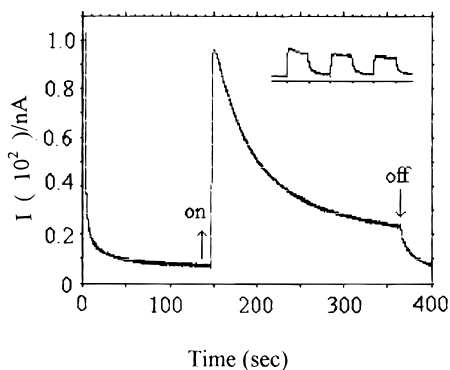


**Figure 5.** Photoelectric response of AI-SnO<sub>2</sub>, deposited from 0.1 mol/L NaI aqueous solution subphase, in 1 mol/L KCl electrolyte solution under an irradiation of 10 mW/cm<sup>2</sup>.

**Comprehensive Effect of Favorable Factors.** From the above results, it can be seen that negative bias voltage, electron acceptor, and the concentration of O<sub>2</sub> in electrolyte solution are all positive factors in enhancing the photocurrent. To test whether these factors produce contradictory contributions to the photocurrent when they are applied simultaneously, we selected the above positive factors. It is interesting to find that for the four independent testing samples, the photocurrent may be enhanced 8 times when the conditions of -100 mV bias, 8 mM MV<sup>2+</sup> in 1 mol/L KCl electrolyte solution, and O<sub>2</sub>-saturated electrolyte solution were used than that resulting from 1 mol/L KCl electrolyte solution only. As a result, the quantum yield at 450 nm reached about 0.9–1.1%.

**Effect of I<sup>-</sup> and the Layer Numbers of AI.** From the discussion of the Langmuir-Blodgett deposition, we found that I<sup>-</sup> ions occupy a certain area in the formation of the film. The presence of I<sup>-</sup> ions in the LB film makes the photocurrent generation much different from the photocurrent generated from the AI-SnO<sub>2</sub> electrode deposited from pure water subphase. Under a lower irradiation power 10 mW/cm<sup>2</sup>, a peak current (~900 nA) following a gradual decreasing to reach a steady value (~240 nA) was observed as shown in Figure 5. After that, only the steady value can be repetitive without the instantaneous peak current. The addition of electron acceptor MV<sup>2+</sup> cannot help to obtain a stable photocurrent for every new LB film of AI deposited from 0.1 mol/L NaI aqueous subphase. Since there are no I<sup>-</sup> ions in electrolyte solution, I<sup>-</sup> ions may diffuse to the electrobilayer at the interface between the electrode and the electrolyte solution to reach an equilibrium slowly and consequently, the photocurrent may reach a steady state gradually. On the basis of this idea, 1 mol/L NaI was used as electrolyte solution, the peak photocurrent still appeared for every new AI LB films containing I<sup>-</sup> ions, but the magnitude of the steady photocurrent is larger than that in 1 mol/L KCl electrolyte solution. The reason may be that I<sup>-</sup> ions in LB film can decrease the film resistance. When some MV<sup>2+</sup> is added to the 1 mol/L NaI electrolyte solution to make the concentration of MV<sup>2+</sup> about 10 mmol/L, only one stably steady photocurrent appeared for every new AI LB film containing I<sup>-</sup> ions. The value of the photocurrent reaches about 500 nA for the AI LB film modified SnO<sub>2</sub> electrode under 10 mW/cm<sup>2</sup> irradiation. The quantum yield at 450 nm is about 0.7%. That is a considerable enhancement of the photocurrent compared with the AI-SnO<sub>2</sub> without the presence of I<sup>-</sup> ions.

Since I<sup>-</sup> can enhance the photocurrent from the AI-SnO<sub>2</sub> electrode and improve the film formation properties, multiple layers of LB films were deposited in 0.1 mol/L NaI aqueous subphase. Just like the results mentioned above, there is a high peak photocurrent following a slow decay to reach a saturate

**TABLE 1: Photocurrent Value of Multiple Layers of AI-SnO<sub>2</sub> Deposited from 0.1 mol/L NaI Aqueous Solution under 10 mW/cm<sup>2</sup> Irradiation Using 1 mol/L NaI Electrolyte Solution Containing 10 mmol/L MV<sup>2+</sup>**

no. of layers	1	3	5	7	9
photocurrent (nA)	500	1000	1100	1155	970

**TABLE 2: Electrochemical Data (vs Ag/AgCl) of AI in LB Film in Different pH Electrolyte Solution**

pH	E <sub>c</sub> (V)	E <sub>a</sub> (V)	ΔE (V)
2	0.07	0.24	0.17
4	-0.10	0.11	0.21
6	-0.24	0.02	0.26

photocurrent for all the multiple-layer-modified SnO<sub>2</sub> electrodes in 1 mol/L KCl electrolyte solution. For instance, only a saturate photocurrent of 90–120 nA can be observed for the SnO<sub>2</sub> electrode which was coated with nine layers of AI under 10 mW/cm<sup>2</sup> irradiation in 1 mol/L KCl electrolyte solution. When 1 mol/L NaI aqueous solution together with 10 mmol/L MV<sup>2+</sup> was used to substitute the 1 mol/L KCl electrolyte solution into the electrolyte solution, a stable photocurrent for SnO<sub>2</sub> electrode coated by one layer of about 500 nA under 10 mW/cm<sup>2</sup> irradiation can be obtained. The results are listed in Table 1. The magnitude of photocurrent did not increase with increasing layer numbers after three layers. It may reach a stable value about 1100 nA. As a comparison, three independent testing samples of two-layer modified SnO<sub>2</sub> deposited from pure water subphase in 1 mol/L KCl electrolyte solution give only about 220–280 nA stable photocurrent under an irradiation of 240 mW/cm<sup>2</sup>.

Since AI contains a long alkyl chain, the resistance will increase with the number of layers. That is why the two layers of AI on SnO<sub>2</sub> deposited from pure water subphase without I<sup>-</sup> ions generate a smaller photocurrent than one layer film deposited from 0.1 M NaI aqueous subphase. The presence of I<sup>-</sup> ions in LB films and in electrolyte solution depresses diffuse of I<sup>-</sup> ions from LB film to the electrolyte solution. The increase in the photocurrent may result from the decrease of film resistance.

**Photoelectrochemical Behavior of AI in LB Film.** It is well-known that the redox reaction of azo group must involve two protons.<sup>23,24</sup> Table 2 lists the different electrochemical data of AI in LB film at different pH. From it, one can conclude that the redox process becomes more irreversible with the increase in pH value. When the pH value is larger than 7, the reduction peak cannot be distinguished clearly. Furthermore, with the pH value increasing, the reduction and oxidation potentials shift to negative direction. In each pH value, many cycles of scanning were carried out and the signals were very stable. There is a certain variation of the reduction potential for different film; for example, the E<sub>c</sub> varies from -0.24 to -0.32 V for the films deposited from pure water subphase at different times, while the oxidation potential shows little variation, E<sub>a</sub> = 0.02 V. That may result from the different aggregating states of AI in LB film.

Therefore, the electrode reaction of AI in lower pH value may occur as in Scheme 1.

To better understand the electrochemical behavior of AI in LB film, the relationship between the peak current of reduction or oxidation, I<sub>p</sub>, and the square root of different scan rates has been studied in pH 4.0 B-R buffer solution. At lower scan rates (≤100 mV/s), the peak current of reduction (I<sub>p,red</sub>) is linear to the square root of different scan rates, but it deviates from the linear relationship at higher scan rates while the peak current of oxidation (I<sub>p,ox</sub>) on SnO<sub>2</sub> electrode keeps a good linear relationship to the scan rate in the studied range (20–800 mV/

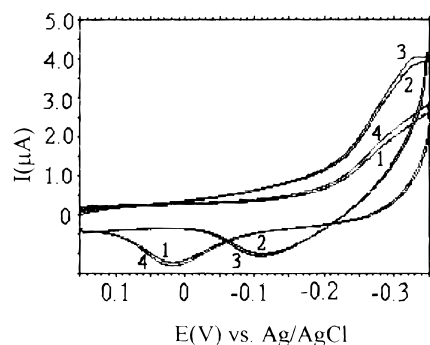


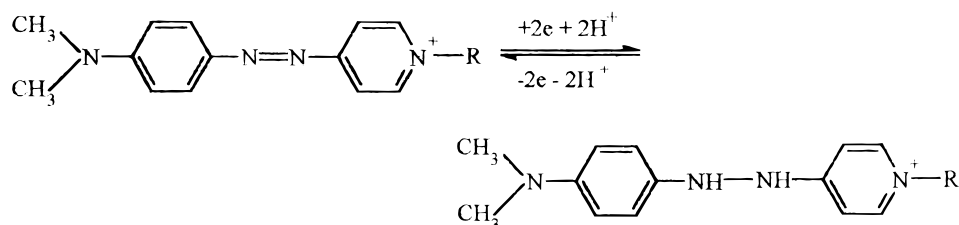
**Figure 6.** Change of CV curves of AI-SnO<sub>2</sub> electrode (1) before irradiation, (2) under irradiation of 240 mW/cm<sup>2</sup>, (3) keeping on irradiation, and (4) switching off irradiation at pH 6 (R-B buffer). Scan rate is 10 mV/s.

s). The linear relationship indicates that the redox reaction of AI in LB film is controlled by electron transfer process. With the increment of scan rate, the difference between the reduction and the oxidation peak position increased in the CV curves from AI-SnO<sub>2</sub> electrode and the process becomes more irreversible.

Unlike other organic materials, AI has no detectable fluorescent properties, so the excited states cannot be studied by using fluorescent characterization. Fortunately, its electrochemical activity provides a new method to detect the excited state when the AI-SnO<sub>2</sub> electrode is illuminated. Figure 6 shows the CV curve of the AI-SnO<sub>2</sub> electrode at pH 6.0 before irradiation and under irradiation of white light of 240 mW/cm<sup>2</sup>. From Figure 6, it can be seen that AI in SnO<sub>2</sub> electrode undergoes a redox process before irradiation due to the redox reaction of azo group. After the light is switched on, the reduction peak current increases and the potential position shows little shift. However, the oxidation peak shows about 130 mV negative shift, e.g.  $E_a$  shifts from 0.02 to -0.11 V, meaning that the excited state is much easier to be oxidized. When the light irradiation is kept on, the shape of the CV curve shows little change, but it recovers to the original state rapidly after the light is switched off. The same results were obtained after repeating more than 10 times. It is interesting that the lower the pH value is, the smaller the negative shift of the oxidation potential.

**Mechanisms of the Photocurrent Generation. Tautomerism of AI in Solution.** Like other solvachromic materials, the difference of the solvent polarity can lead to the absorption variation of AI. In lower polarity solvent, such as benzene, an absorption at 400 nm and an absorption at 540 nm appear

#### SCHEME 1



#### SCHEME 2

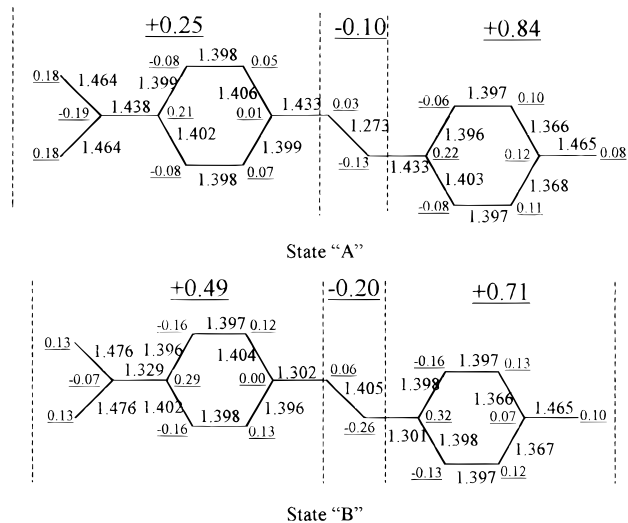
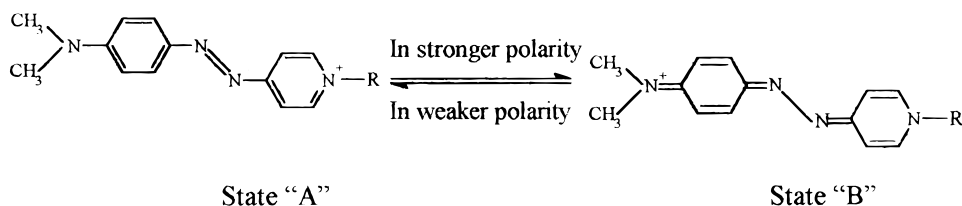


**Figure 7.** Calculated bond lengths (give in Å) and atomic charges (underline, give in +e) of AM molecule skeleton. All hydrogen atomic are omitted for clarity.

simultaneously while there is only one strong absorption at 555 nm in a higher polarity solvent, for example, ethanol. The similar results can be obtained in acetone ( $\lambda_{\max} = 553$  nm) and in chloroform ( $\lambda_{\max} = 560$  nm) solvent. The process may be demonstrated as Scheme 2. Considering the change in Scheme 2, we can infer that AI may exist as a mixture of state A and state B in benzene solvent, but in polar solvent, it may exist as only one structure, state B.

By using the MINDO/3 method based on the assumption of neglecting the interaction of the molecules, the two possible states of simplified molecule, (CH<sub>3</sub>)<sub>2</sub>NC<sub>6</sub>H<sub>4</sub>-N=N-C<sub>5</sub>H<sub>4</sub>N<sup>+</sup>-CH<sub>3</sub> (AM), have been calculated. The positive charge distribution and fitting bond length of AM corresponding to the lowest total energy after optimization are shown in Figure 7.

From MINDO/3 calculations, the dipole moments of state A and state B are 15.16 and 4.38 D, respectively. Data also show that the bond lengths are quite different in the two states. In state B, all the bond lengths are nearly uniform; for instance, the bond lengths of ph-N-N-py for state A are 1.443, 1.273, and 1.433 Å, respectively. Conversely, in state B, they are 1.302, 1.405, and 1.301 Å. Although both state A and state B bear a net positive charge, the electrons of state B delocalized much stronger than that of state A, suggesting that state B has a larger  $\pi$ -conjugate system than state A. Consequently, a



is generated from photoinduced tautomerism other than *trans*–*cis* isomerism. The unification between experimental data and calculation results shows that the above assumption of neglecting the interaction of the molecules does not lead to much error and is indicative of the proposed mechanism.

**Electron Transfer Mechanisms on AI–SnO<sub>2</sub> Electrode.** From the absorption spectrum change of AI in benzene solvent when the solution is illuminated, a tautomerization takes place upon irradiation and follows a first-order kinetic process after illumination under dark. However, when the floating AI was transferred from the air–water interface to the SnO<sub>2</sub> substrate, the tautomerization cannot be observed using the conventional UV–vis absorption method. This phenomenon may result from the strong interaction among the chromophores in the organized packing of the LB film, therefore resulting in the rapid decay process from excited state. However, it can be observed clearly by using cyclic voltammetry under irradiation. The recovery of the CV curve to the original state rapidly after irradiation (see Figure 9) is good support of that conclusion.

The flatband potential ( $\phi_{fb}$ ) of SnO<sub>2</sub> is  $-0.34V^{25}$  (vs SCE) at pH 6. When Ag/AgCl electrode is used as reference, the flatband potential is about  $-0.32 V$ . In the present study, the reduction and oxidation potentials are  $-0.32 V$  and  $0.02 V$  (vs Ag/AgCl), respectively, before irradiation at pH 6. After irradiation the redox process become more reversible:  $E_a = -0.13 V$  and  $E_c = -0.32 V$  ( $\sim$ Ag/AgCl) as shown in Figure 6. The appearance of more negative oxidation potential of the excited state makes it easier to give out electrons than that for the ground state. The reversible redox signals of AI on SnO<sub>2</sub> electrode under irradiation may result from the excited state, probably state B. Based on the oxidation potential of AI aggregates ( $\sim 0.02 V$ , vs Ag/AgCl), the oxidation potential of excited AI aggregates ( $\sim -0.13 V$ ,  $\sim$ Ag/AgCl), and the energy level of the SnO<sub>2</sub> electrode, a probable mechanism for this conductive process can be shown in Scheme 4.

The reduction potential of MV<sup>2+</sup> is  $-0.10 V$  (vs Ag/AgCl) in the present study at pH 6, close to the oxidation potential of the AI excited state. It is reasonable for MV<sup>2+</sup> to act as an effective electron acceptor and enhance the cathodic photocurrent. Conversely, strong donors such as AA and HQ cannot enhance the cathodic photocurrent probably because their energy does not match the energy level of the excited AI on SnO<sub>2</sub>. Because the oxidation potential of HQ is about  $-0.05 V$  (vs Ag/AgCl) at pH 6 and that of AA is about  $0.10 V^{26}$  ( $\sim$ Ag/AgCl) which are higher than the reduction potential of AI, the electron transfer from HQ to AI is impossible. Many reports<sup>13,27–29</sup> indicate that O<sub>2</sub> may play a vital role in the electron transfer process through accepting an electron to form a superoxide radical. In the present AI–SnO<sub>2</sub> system, O<sub>2</sub> can enhance the photocurrent as an electron acceptor probably through the same mechanism. However, when the electrolyte solution is degassed by N<sub>2</sub>, it does not decrease in a large scale ( $<5\%$ ). From this fact, it is easy to think that O<sub>2</sub> is a helpful factor to the photocurrent, but it is not a decisive one at ambient condition.

## Conclusion

The present data from both experiments and theoretical calculations suggest that the cathodic photocurrent is generated from the excited state AI. The mechanism is also supported by studying the effect of bias voltage, the addition of the donors and acceptors, and light intensity on the photocurrent generation. The addition of I<sup>–</sup> ions can enhance the photocurrent to a large scale. The quantum yield is 0.14% at ambient condition and it can be raised to 1.0% at optimal conditions. I<sup>–</sup> ions also

improve the quantum yield with the help of electron acceptor in electrolyte solution with a quantum yield about 0.7%. All these results indicate that AI is an ideal material to be used in the field of photogenerated charge storage, photoelectric conversion, and other photoelectronic devices. In addition, the behavior of the novel dye AI also provides a set of basic data for designing and finding other more effective photoelectronic materials.

**Acknowledgment.** The authors thank the National Climbing Plan A and B and the National Natural Science Foundation of China for financial support of this project.

## References and Notes

- (1) Kotov, N. A.; Kuzmin, M. G. *J. Electroanal. Chem.* **1992**, *341*, 47.
- (2) Ivanov, I., Ed. *Thin Liquid Films*; Marcel Dekker: New York, 1988; pp 827–1057.
- (3) Tien, H. Ti. *Prog. Surface Sci.* **1992**, *41*, 337.
- (4) Fujihira, M. *Nanostructure Based Molecular Materials*; Geopel, W., Ziegler, C., Eds.; VCH: Weinheim, Germany, 1992; pp 27–46.
- (5) For example: (a) Nábauer, A.; Berg, P.; Ruge, I. *Nanostructure Based Molecular Materials*; Geopel, W., Ziegler, C., Eds.; VCH: Weinheim, Germany, 1992; pp 72–78. (b) Kuhn, H. *Thin Solid Films* **1989**, *178*, 1.
- (6) For example: (a) Ashwell, G. J., Ed. *Molecular Electronics: Research Studies*; John Wiley & Sons: New York, 1992. (b) Carter, F. L., Ed. *Molecular Electronic Devices*; Dekker: New York, 1983.
- (7) For example: (a) Moser, C. C.; Keske, J. M.; Warncke, K.; Farid, R. S.; Dutton, P. L. *Nature* **1992**, *335*, 796. (b) Kakitani, T.; Mataga, N. *J. Phys. Chem.* **1988**, *92*, 5059.
- (8) For example: (a) Trans-Thi, T. H.; Lipskier, J. F.; Houde, D.; Pepin, C.; Keszei, E.; Jay-Gerin, J.-P. *J. Chem. Soc., Faraday Trans.* **1992**, *88*, 2129. (b) Willig, F.; Eichberger, R.; Bitterling, K.; Durfee, W. S.; Stock, W. *Ber. Bunsenges. Phys. Chem.* **1987**, *91*, 867. (c) Sakomura, M.; Fujihira, M. *Thin Solid Films* **1994**, *243*, 616. (d) Macdowell, L. M.; Kirmaier, C. Holten, D. *J. Phys. Chem.* **1991**, *95*, 3379.
- (9) (a) Naito, K.; Miure, A. *J. Am. Chem. Soc.* **1993**, *115*, 5185. (b) Naito, K.; Miure, A. *Thin Solid Films* **1994**, *242*, 191.
- (10) Fujihira, M. *New Functionality Materials. Vol. C. Synthetic Process and Control of Functionality Materials*; Tusurta, T., Doyama, M., Seno, M., Eds.; Elsevier Science Publishers B. V.: Amsterdam, 1993; pp 473–480.
- (11) For example: Saito, K.; Yokoyama, H. *Thin Solid Films* **1994**, *243*, 526.
- (12) Fujihira, M.; Sakomura, M. *Thin Solid Films* **1989**, *179*, 471.
- (13) Kim, K.-s.; Liang, K.; Law, K.-Y.; Whitten, D. G. *J. Phys. Chem.* **1994**, *98*, 984.
- (14) For example: Fujihira, M.; Aoki, K.; Inowe, S.; Takemura, H.; Muraki, A.; Aoyagui, S. *Thin Solid Films* **1985**, *132*, 221.
- (15) Liu, Z. F.; Hashimoto, K.; Fujishima, A. *Nature* **1990**, *347*, 658.
- (16) Li, H.; Huang, C. H.; Zhou Y. F. Zhao, X. S.; Xie, X. H.; Li T. K.; Bei J. *J. Mater. Chem.* **1995**, *5* (11), 1871.
- (17) Tachibana, H.; Nakamura, T.; Matsumoto, M.; Komizu, H.; Manda, E.; Niino, H.; Yabe, A.; Kawabata, Y. *J. Am. Chem. Soc.* **1989**, *111*, 3080.
- (18) Li, H.; Huang, C. H.; Zhao, X. S.; Xie, X. M.; Xu, L. G.; Li, T. K. *Langmuir* **1994**, *10*, 3794.
- (19) Matsuo, T.; Itoh, K.; Takuma, K.; Hashimoto, K.; Nagamura, T. *Chem. Lett.* **1980**, 1009.
- (20) Tien, H. Ti. *Bilayer Lipid Membranes, Theory and Practice*; Marcel Dekker: New York, 1974.
- (21) Machae, E. G.; Kasha, M. *Physical Processes in Radiation Biology*; Academic Press: New York 1964; p 23.
- (22) Morov, S. L. *Handbook of Photochemistry*; Marcel Dekker: New York, 1973; p 89.
- (23) Liu, Z. F.; Loo, B. H.; Hashimoto, K.; Fujishima, A. *J. Electroanal. Chem.* **1991**, *297*, 133.
- (24) Xia W. S.; Huang C. H.; Ye X. Z.; Luo C. P.; Gan L. B.; Liu Z. F. *J. Phys. Chem.* **1996**, *100*, 2244.
- (25) Mollers, F.; Memming, R. *Ber. Bunsenges. Phys. Chem.* **1972**, *76*, 469.
- (26) Meites, L.; Zuma, P.; Rupp, E., Eds. *CRC Handbook Series in Organic Electrochemistry*; CRC Press: Boca Raton, FL, 1983; Vol. 4.
- (27) Haraguchi, A.; Yonezawa, Y.; Hanawa, R. *Photochem. Photobiol.* **1990**, *52*, 307.
- (28) Hada, H.; Yonezawa, Y. *Synth. Met.* **1987**, *18*, 791.
- (29) Hada, H.; Yonezawa, Y.; Inaba, H. *Ber. Bunsenges. Phys. Chem.* **1981**, *85*, 425.